Intraoperative transesophageal echocardiography: the roadmap for successful mitral valve repair

Anand R. Mehta[1,2], **Nelson Burbano-Vera**[1,3]

[1]Division of Cardiothoracic and Vascular Anesthesiology, Department of Anesthesiology, Integrated Hospital-Care Institute, Cleveland Clinic, Cleveland, OH, USA; [2]Department of Anesthesiology, Cleveland Clinic Lerner College of Medicine of Case Western Reserve University, Cleveland, OH, USA; [3]Section of Pediatric Cardiac Anesthesiology, Division of Pediatric Anesthesiology, Department of Integrated Surgical Care, Children's Institute, Cleveland, OH, USA

Correspondence to: Anand R. Mehta, MD, FASE. Staff Anesthesiologist, Division of Cardiothoracic and Vascular Anesthesiology, Department of Anesthesiology, Integrated Hospital-Care Institute, Cleveland Clinic, 9500 Euclid Avenue, Cleveland, OH 44195, USA; Associate Professor of Anesthesiology, Cleveland Clinic Lerner College of Medicine of Case Western Reserve University, Cleveland, OH, USA. Email: mehtaa2@ccf.org.

Intraoperative transesophageal echocardiography (TEE) is crucial in defining a real-time imaging guide for a successful surgical repair of degenerative mitral valve (MV) disease. Three-dimensional TEE enhances the echocardiographer's ability to delineate and communicate the pathology more precisely. It is an invaluable tool in guiding peripheral cannulation for minimally invasive and robot-assisted surgical valve repairs and is critical in determining the adequacy of repair and associated complications. As an imaging modality, TEE is an indispensable aid during mitral valve repair (MVR).

Keywords: Degenerative mitral valve disease; mitral valve repair (MVR); transesophageal echocardiography (TEE)

Submitted Aug 27, 2025. Accepted for publication Jan 22, 2026. Published online Jan 29, 2026.
doi: 10.21037/acs-2025-dmv-10
View this article at: https://dx.doi.org/10.21037/acs-2025-dmv-10

Introduction

Technological advances in transesophageal echocardiography (TEE) have rendered intraoperative TEE essential for mitral valve repair (MVR). TEE provides precise dynamic information of the mitral valve (MV) structure and function, enabling the most appropriate repair for a particular pathology. In short, TEE provides a "surgical road map" for MV surgery (1) (*Video 1*).

Structural anatomy of the MV

The mitral annulus (MA), leaflets, chordae tendineae (CT), and papillary muscles form a highly complex structure called the MV apparatus that prevents mitral regurgitation (MR) and maintains the left ventricular geometry and function (*Figure 1*) (2). The MA is saddle-shaped with a shorter anteroposterior diameter (APD) and a larger commissural diameter. The anterior part of the annulus is higher than the posterior, with its lowest portions at the commissures. This nonplanar shape of the annulus reduces the stress on the leaflets considerably (2). Anteriorly, it is flanked by the left trigone (LT) and right trigone, bridged by the intervalvular fibrosa (IVF), forming the continuity between the mitral and the aortic valves (3). The left coronary and non-coronary aortic cusps are adjacent to the IVF, and the coronary sinus and the left circumflex artery (LCX) to the posterior annulus (4,5). These spatial relationships are important to assess damage to these structures during MV surgery (6). The CT are connected to the anterolateral (AL) and posteromedial (PM) papillary muscles. The non-contractile chords accommodate the contractile stress of the papillary muscles, permitting valve closure and preventing prolapse of the mitral leaflets during systole. The primary (marginal) chords maintain leaflet apposition during systole and the secondary (basal) chords maintain the left ventricular geometry (2,7). The posterior leaflet has a larger circumferential (two-thirds compared to one-third for the anterior leaflet) attachment to the annulus and has indentations called scallops, which help to accommodate

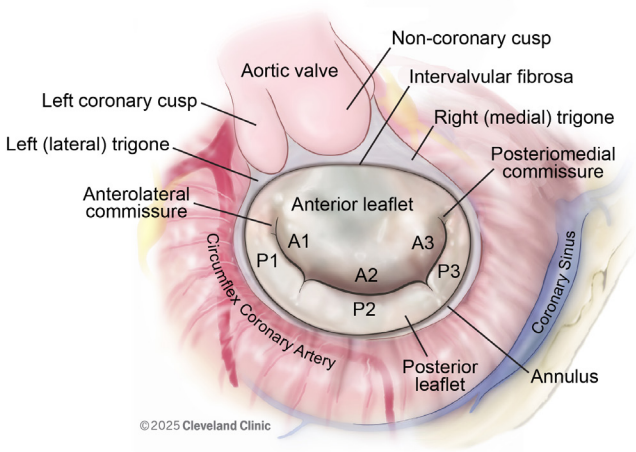

Figure 1 Mitral valve anatomy.

the smooth, streamlined anterior leaflet along a curvilinear coaptation line (CL) (7,8). The CL is flanked by the AL commissure (ALC) (9) close to the left atrial appendage and the LT, and the PM commissure (PMC) adjacent to the right trigone. The commonly used Carpentier's nomenclature divides the posterior leaflet into 3 scallops P1, P2 and P3. The P1 scallop is adjacent to the ALC and the left atrial appendage and is anterior, lateral and superior. The P3 scallop is closer to the PMC and is posterior, medial and inferior. The middle scallop P2 lies between P1 and P3 (7). The P2 scallop is the most commonly diseased segment in fibroelastic deficiency (FED) (10). The anterior leaflet is without scallops and is divided into 3 segments, A1, A2 and A3, corresponding to the respective posterior segments. Duran also divided the posterior segment into two segments (P1, P2 and P3), however, the anterior segment was described as two segments: A1 (medial) and A2 (lateral). Additionally, he also described 2 commissural segments C1 (AL) and C2 (PM) (11).

Degenerative mitral valve regurgitation (DMR)

DMR is a spectrum of abnormalities ranging from segmental involvement to multi-segment afflictions accompanied by significant annular dilatation. FED is on the isolated spectrum of the disease, involving usually the P2 segment, whereas Barlow's disease (BD), also referred to as diffuse myxomatous disease (DMD), represents a more diffuse disease, both characterized by either prolapse or flail of the affected segments (*Figure 2*) (10,12). "The functional approach" by Carpentier classifies MR into 3 types based on the effect of the pathophysiology on leaflet motion (LM). Type I is characterized by normal, type 2 excessive and type 3 restricted LM. Type 3 has been further classified as A and B based on restriction in both systole and diastole or systole alone (13). DMR represents type 2 abnormality. Sidebotham and colleagues have described a type 4 as LM associated with systolic anterior motion (SAM), which is further subclassified as 4a associated with hypertrophic cardiomyopathy, 4b as post repair SAM and 4c as hemodynamically induced SAM. They also describe a type 5 related to hybrid conditions such as restriction of the posterior leaflet in conjunction with prolapse of the anterior leaflet (9).

DMD demonstrates myxomatous changes with mucopolysaccharide accumulation in the mucosa of the valve. The chords are commonly thickened, fused and often calcified. In the FED, there is a deficiency rather than an excess of connective tissue. The prolapsing segment may demonstrate thickening because of secondary myxoid deposition. Forme fruste (atypical or incomplete) describes valves with some but not all features of BD, thus defining a spectrum of disease process (10). The severity of MR in DMD varies from mild to severe and is in mid to late systole, as compared to FED, in which it is usually severe and holosystolic (3,10,14). Morphologically, the presence of a flail segment is associated with severe MR (15). The diffuse nature of the disease with DMD requires a more complex surgical repair as compared to the isolated lesions in FED (3,14). Excessive movement of the leaflet associated with a prolapse into the LA by a margin of ≥2 mm from the MA is characteristic (16).

Three-dimensional echocardiography (3DE) has resulted in better comprehension of the MV in DMR. Normally, in early systole, there is a decrease in the APD of the annulus and an apical descent of the commissures because of the contraction of the papillary muscles, further accentuating the saddle shape of the MA. The MA in DMR is enlarged, flattened and more circular with increases in both diameters, circumference and valve area. The annular enlargement is more severe with DMD than FED. In FED, the annular dynamics are close to normal whereas in DMD there is an absence of the anteroposterior contraction with no deepening in the saddle shape with an abnormal enlargement in late systole suggestive of annular involvement. Leaflet redundancy is more pronounced with DMD than FED with larger leaflet areas and prolapse volume which may be beneficial in covering the annular area in systole limiting the severity of MR. DMR associated with

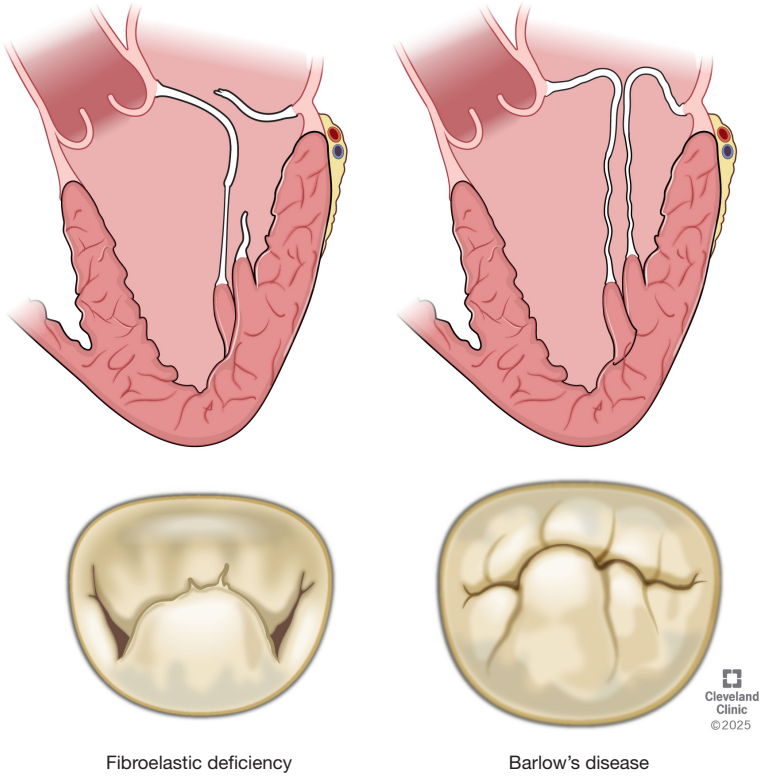

Figure 2 Fibroelastic deficiency & Barlow's disease.

mitral annular calcification (MAC) may render MVR more difficult (14). Cleft like indentations are common with DMR due to an increase in leaflet tissue and can lead to post-repair residual MR if not addressed. Deep clefts are defined as indentations extending more than 50% of the leaflet and seen adjacent to the prolapse or flail segments (17). Some believe that as the prolapse increases, these may represent a prominence between the diseased and the normal segment. These clefts are better visualized with 3DE as compared to two-dimensional echocardiography (2DE) (18).

A comprehensive TEE examination with emphasis on the MV is key to a successful MVR. Intraoperatively, TEE is an ideal real time (RT) imaging modality as the MV and LA, being closest to the esophagus, provide excellent windows. This also allows imaging at higher frequencies and shallower depths resulting in higher spatial and temporal resolution. Since the atrial surface of the valve lies in the near field, acoustic shadowing caused by MAC or prosthetic material do not interfere with imaging. Thus, TEE is superior to transthoracic echocardiography (TTE) for MV abnormalities (8). The initial assessment is aimed at identifying the mechanism, severity of MR, repairability, other valvular abnormalities, ventricular systolic function, the risk of SAM after repair (9,19,20). and a guide for cannulation and device placement for minimally invasive and robot-assisted MV surgery (21). TEE may influence the surgical approach for MVR. Presence of moderate to severe aortic regurgitation, severe MAC, left ventricular dysfunction, or pulmonary hypertension may steer a surgeon towards choosing the sternotomy approach (22).

Two-dimensional (2D) TEE examination

The MV can be visualized from the mid-esophageal (ME) and transgastric (TG) views (*Figure 3*). The 5-ME views are obtained by motoring the multiplanar angle from 0 to 180°. The ME 4-chamber view (0–10°) demonstrates the A3A2-P2P1 segments, the ME commissural view (50–70°) demonstrates the P1-A3A2A1-P3 segments, the ME 2-chamber view (0–90°) demonstrates the P3-A1A2A3 segments and the ME LAX view (120–140°) demonstrates the P2-A2 segments. Retroflexing or withdrawing the probe from the 4-chamber view, a 5-chamber view (0–

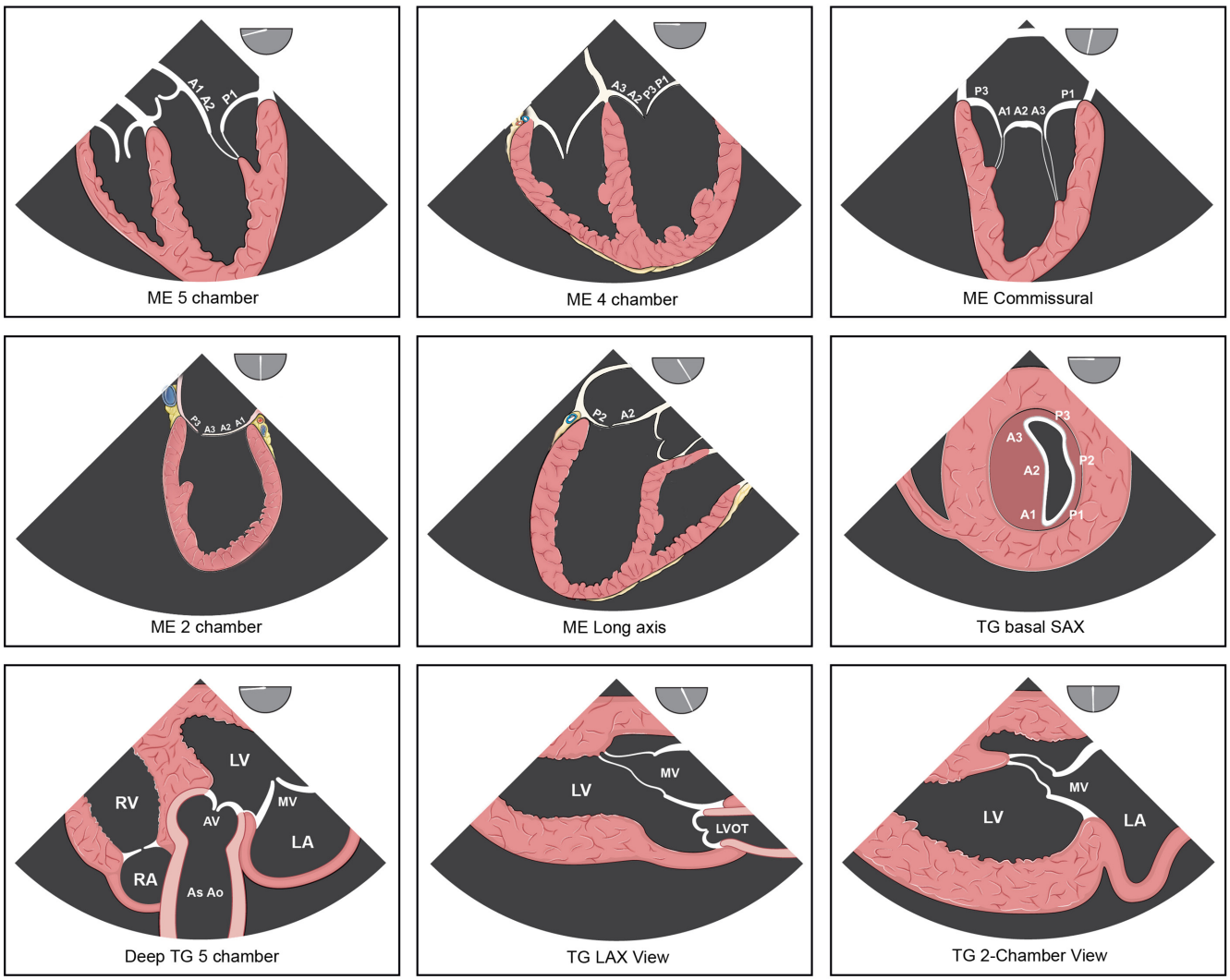

Figure 3 ME & TG 2D TEE views of the mitral valve. 2D, two-dimensional; LAX, long axis view; ME, midesophageal; SAX, short axis view; TEE, transesophageal echocardiography; TG, transgastric.

10°) can be obtained which demonstrates the A2A1-P1 segments (8). 2D TEE is often limited by the ambiguity created by probe and sector rotation leading to a variable description of the observed segments in the ME views. A 3D TEE examination overcomes this limitation with a more precise segmental identification (9). The TG basal view (0–20°) demonstrates the MV in its short axis (SA). The TG 2-chamber view (90–110°) is useful in discerning abnormalities of the sub valvular apparatus (23). The MV in the TG LAX (120–140°) and the deep TG view (0–20°) lie in the far field limiting their utility.

Color flow Doppler (CFD) interrogation of the MV in DMR reveals the severity and the mechanism responsible for MR. Both prolapse and flail direct the flow away from the diseased segment (24). P1 abnormalities can be an exception as it lies close to the ALC, which is relatively anterior. Therefore, P1 pathology may direct the flow posteriorly rather than anteriorly (25). With more complex segmental involvements with both restriction and excessive LM present in different segments of the MV, the jet direction is dictated by the predominant lesion. This is more commonly seen in patients with mixed etiologies such as patients with a prolapse or flail segments who develop myocardial infarction with functional MR resulting from

concomitant tethering (16).

Severity of MR should be adjudicated on an integrated approach rather than relying on a single measure, as each individual measurement may demonstrate variability and may not have the same predictive value in different circumstances (16).

CFD, though essential for identifying MR, is not very reliable in grading its severity (26). Regurgitant jet area (JA), even when indexed for the size of the LA, can vary with changes in blood pressure (BP). Higher BP can increase its severity whereas lower pressures can produce a smaller JA. Changes in loading conditions under anesthesia may significantly underestimate the severity of MR (19). Pharmacological challenges to increase the BP help gauge the true severity of MR (27,28). The severity of eccentric jets seen with flail segments is underestimated by JA (29). The ASE recommends a Nyquist limit of 50–70 cm/s while interrogating native valve regurgitant lesions. Lowering the Nyquist limit would result in the jet appearing larger and vice versa (16).

M-mode echocardiography has exceptional temporal resolution. Color M-mode provides information regarding the timing and duration of the jet in systole. Early brief jets are usually mild whereas pansystolic jets are severe (16).

The vena contracta (VC) is the narrowest portion of the jet at or immediately downstream from the regurgitant orifice (RO). Measurement of the VC width (VCW) and area (VCA) is useful in assessing the severity of MR (19,30). The VCA represents the effective regurgitant orifice area (EROA). VCW is dependent on the geometry of the RO and could underestimate the severity in elliptical orifices (secondary MR) or with multiple jets (16). Multiplanar reconstruction (MPR) on 3DE allows the direct measurement of the VCW and VCA (31).

The EROA can be calculated using Doppler echocardiography by the proximal isovelocity surface area (PISA) method. This method is based on the combined principles of the properties of flow dynamics and the continuity principle (32). The PISA method also enables the calculation of the regurgitant volume (RV) and regurgitant fraction (RF) (32,33).

The PISA evaluation in MR is more accurate for central jets as compared to eccentric jets.

Continuous wave Doppler (CWD) interrogation provides valuable qualitative information about MR. A high-pressure gradient between the left ventricle and atrium translates into a maximum MR jet velocity of 4–6 m/s. A lower velocity may reflect poor ventricular function or an elevated left atrial pressure. A dense CWD signal and a truncated triangular jet with an early peaking velocity is suggestive of severe MR.

The RV and RF can also be calculated as the difference between MV stroke volume (SV) and left ventricular outflow tract (LVOT) SV, provided there is no aortic regurgitation. RF is calculated by dividing the RV by the SV. Both RV and RF can also be calculated as the difference between the total SV as measured by 2DE or 3DE and LVOT SV. 2DE tends to underestimate the SV and thus is less accurate than 3DE. RV, RF and EROA are quantitative estimates of the severity of MR and are better predictors of outcome (*Table 1*) (16).

Reversal of pulmonary vein flow (PVF) in more than one pulmonary vein (PV) is very specific for severe MR (34). Lesser degrees of MR may result in blunting of PVF. All four PV may not demonstrate flow reversal, as this finding is dictated by the direction of flow (35).

Additionally, chronicity of DMR may lead to increases in LA and LV chamber dimensions.

RT TEE also provides a guide for cannulation for establishing peripheral cardiopulmonary bypass (CPB) and detecting complications during robotic and a right thoracotomy approach for MVR (*Figure 4*) (21,36,37).

The cannulae are placed using the Seldinger technique (38). Venous cannulae (VC) are placed via the femoral vein and/ or the right internal jugular (RIJ) vein. For isolated MV procedures, a single femoral venous cannula may suffice with its tip placed in the superior vena cava (SVC). Additionally, an SVC cannula can be placed via the RIJ vein for inadequate drainage. Concomitant procedures on the right heart structures (tricuspid valve repair, atrial septal defect closure) require separate cannulation of the SVC and inferior vena cava (IVC) (38). The tip of the IVC cannula should be at the IVC right atrial (RA) junction and the SVC cannula at the SVC RA junction. Venous cannulation is guided by using the ME bicaval view (90–110°). The guide wire must always be visualized in the RA during cannulation as it tends to get pulled back during dilatation and advancement of the VC. The devices should be visualized along their path from the intrahepatic IVC into the RA to recognize misdirection into the hepatic vein. Injury during venous cannulation can lead to cardiac tamponade (39). Injury to the intrahepatic IVC is seen as fluid around the liver or in the abdomen which is visualized by turning the probe to the right from the TG mid papillary view (0°). The guide wire and the cannula can traverse the interatrial septum during cannulation leading

Table 1 Severity of mitral regurgitation

Parameters	Mild	Moderate	Severe
LA & LV size	Normal	Normal/mildly dilated	Dilated
Jet area (color flow Doppler)	Small, central, narrow, brief	Variable	Large central jet or eccentric wall impinging jet
Flow convergence	Small or transient or absent	Intermediate in size and duration	Large holosystolic
Jet contour on CWD	Faint, partial, parabolic	Dense but partial or parabolic	Holosystolic, dense, triangular
Vena contracta width (cm)	<0.3	0.3–0.6	≥0.7
Pulmonary vein flow	Normal	Normal or blunted	Absent systolic flow or flow reversal
EROA (cm^2)	<0.2	0.2–0.39	≥0.4
Regurgitant volume (mL)	<30	30–59	≥60
Regurgitant fraction (%)	<30	30–49	≥50

Modified from the ASE/SCA recommendations for Non-Invasive Evaluation of Native Valvular Regurgitation (16). ASE, American Society of Echocardiography; CWD, continuous wave Doppler; EROA, effective regurgitant orifice area; LA, left atrium; LV, left ventricle; SCA, Society of Cardiovascular Anesthesiologists.

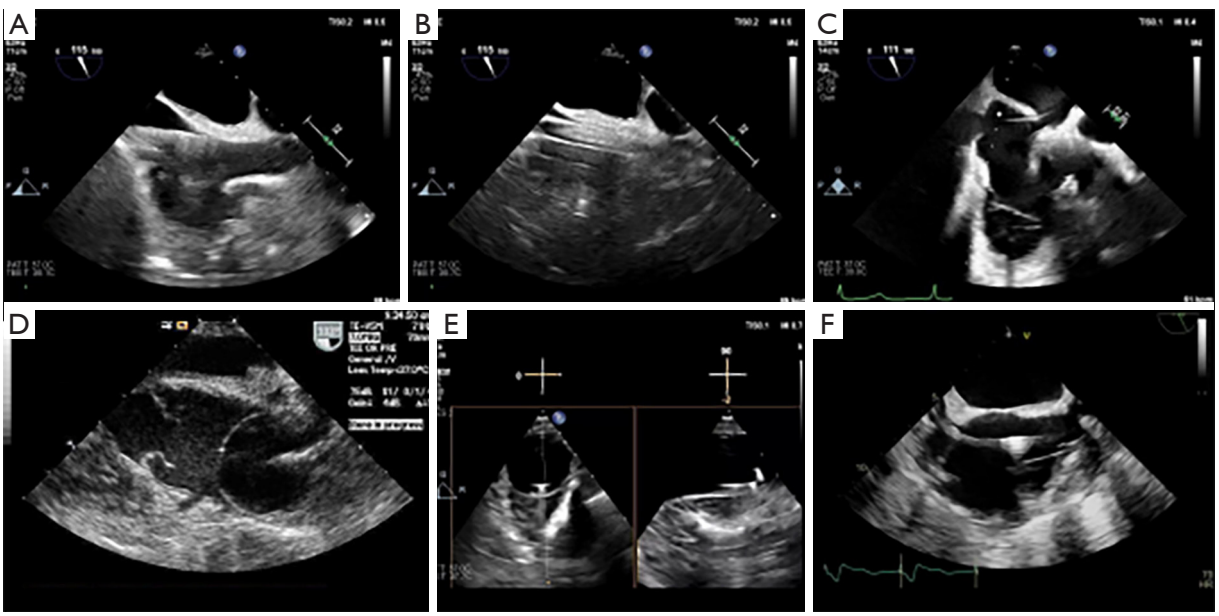

Figure 4 Cannulation & device placement during robotic MV surgery. (A) GW in RA; (B) femoral venous cannula in RA; (C) GW across interatrial septum; (D) endoballoon in the ascending aorta; (E) GW in the descending aorta; (F) percutaneous retrograde coronary sinus catheter. GW, guidewire; MV, mitral valve; RA, right atrium.

to damage to the interatrial septum.

Although the femoral or iliac arterial vessels cannot be visualized by TEE, documenting the presence of the guidewire in the distal descending aorta with TEE is advised prior to advancing the femoral arterial cannula (40). The descending aorta short (0–10°) and LAX (90–100°) views are most commonly used. Screening the visualized descending aorta for atherosclerotic disease is advised to prevent retrograde embolization with severe atherosclerosis. Following arterial cannulation and establishment of CPB,

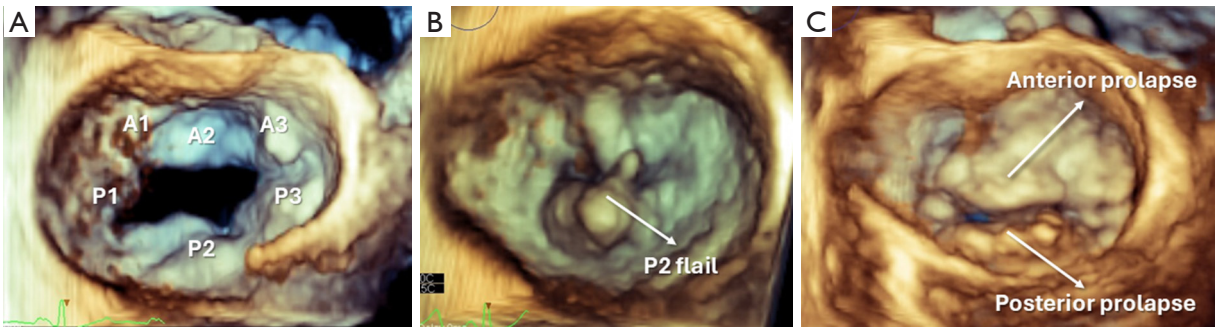

Figure 5 Echocardiographic anatomy of the MV. (A) 3D TEE en-face image from the left atrium perspective (surgical view), showing the lateral (A1), middle (A2) and medial (A3) segments of the anterior mitral leaflet; and lateral (P1), middle (P2) and medial (P3) scallops of the posterior mitral leaflet. (B) 3D TEE surgical view, demonstrating a flail middle scallop (P2) of the posterior leaflet of the MV with ruptured chords in fibroelastic deficiency. (C) 3D TEE surgical view, showing bileaflet prolapse in Barlow's disease. 3D, three-dimensional; MV, mitral valve; TEE, transesophageal echocardiography.

TEE is crucial in detecting an iatrogenic retrograde dissection.

TEE also plays an essential role in placement of the EndoClamp aortic catheter (Edwards Lifesciences, Irvine, CA, USA) which is used to occlude the ascending aorta and to deliver antegrade cardioplegia. Prior to placement it is imperative to screen the ascending aorta for significant atherosclerotic disease (37). The EndoClamp may not be able to achieve total occlusion in an ascending aorta with a diameter in excess of 3.5 cm (21,39). Ascending aortas with a smaller diameter may lead to distal endoballoon migration on inflation. The aortic root and the proximal ascending aorta are best visualized in the ME aortic valve LAX view (120–140°) and the mid ascending aorta is best visualized in the ME ascending aorta LAX view (90–110°) and the mid ascending aorta SA view (0–30°). The device is deployed via the femoral artery and positioned with its tip just distal to the sinotubular junction about 2–4 cm above the sinuses of Valsalva (40). Proximal (aortic valve, coronary arteries, ventricle) or distal (brachiocephalic trunk with cerebral hypoperfusion) migration of the device can be detected with TEE (39).

The modified ME bicaval view (90–110°), modified ME 4-chamber view (0°, advance the probe from the 4-chamber view and turn it to the right) and the "double barrel" (110–140° increasing the multiplanar angle from ME bicaval view) views are key in placing percutaneous coronary sinus catheter (CSC) via the RIJ vein (41). The CSC should be positioned at a depth of at least 4–5 cm in the sinus (42). In the ME 2-chamber view, the CSC catheter can be visualized to the left of the screen. Bi-plane imaging is recommended and can be very useful while placing all the above devices.

The ME bicaval view (90–110°), ME RV inflow-outflow view (50–70°) and the ME ascending aorta SAX view (0–30°) are useful in placing the pulmonary artery (PA) vent in the main PA (43).

Three-dimensional (3D) TEE

3D TEE of the MV represents a major innovation in perioperative cardiovascular ultrasound (44). Realistic, high resolution, RT 3D images of the MV can be acquired with consistent ease. In DMR, 3D TEE is superior in identifying anterior leaflet pathology and segmental analysis of the posterior leaflet compared to 2D, 3D TTE and 2D TEE (45).

3D depth-specific techniques (zoomed-in) are the most frequently used 3D TEE modalities to image the MV. To facilitate anatomic orientation, 3D TEE en-face imaging from the left atrial perspective (surgical view) has become the preferred form to display and communicate MV pathology with the surgical team (46) (*Figure 5A*, *Video 2A*). Diagnostic location of segmental leaflet disease (prolapse and/or flail) and identification of the origin of the MR jet/s in DMR are easily accomplished from this view (*Figure 5B*,*5C*, *Video 2B*,*2C*). Additionally, the 3D image can be rotated independently along all three axes and presented from any desired spatial perspective. Diagnosis of leaflet and commissural pathology, and the direction of the MR jet, are more evident with the 3D TEE modified en-face AL and PM views (47) (*Figure 6A*,*6B*, *Video 3A*,*3B*). The 3D TEE inverted en-face view from the ventricular perspective, when combined with CFD, is useful

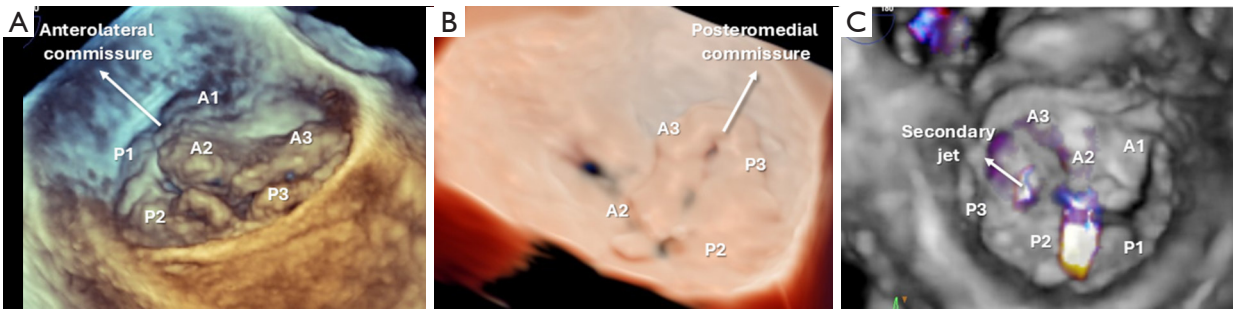

Figure 6 Modified en-face views of the mitral valve. (A) 3D TEE modified en-face posteromedial view from the LA perspective, demonstrating bileaflet prolapse. The direction of view is from the posteromedial toward the anterolateral commissure. (B) Tissue realistic 3D TEE modified en-face anterolateral view from the LA perspective, showing prolapse of A3, P3 and the posteromedial commissure. The direction of view is from the anterolateral toward the posteromedial commissure. (C) 3D TEE color flow Doppler modified en-face view from the left ventricle perspective, demonstrating two jets of MR. The secondary jet of MR located between A3-P3 was obscured by the main jet of MR and not identified from the left atrium perspective. 3D, three-dimensional; LA, left atrium; MR, mitral regurgitation; TEE, transesophageal echocardiography.

in identifying secondary, smaller jets originating from clefts or indentations that may be obscured by a larger primary MR jet observed from the atrial perspective (*Figure 6C*, *Video 3C*). Several postprocessing techniques, such as photorealistic rendering, virtual lighting, simulated light interaction, and translucency enhance the visualization and interpretation of valvular pathology and are especially useful in multisegmented, complex MV pathologies.

MPR of the MV allows simultaneous visualization of 2D and 3D images (48) (*Figure 7A*). Due to technological advances, MPR has evolved into an RT modality for rapid segmental analysis and quantification for MV surgery and structural MV interventions. 3D MPR-based quantification is more precise than 2D measurements as it enables "anatomic certainty" that the structure of interest is being transected in the precise intended tomographic plane. For instance, when measuring A2 segment length in the 2D ME LAX view, it is uncertain whether the tomographic plane exactly transects the middle of the A2 segment. In comparison, MPR allows the plane of interest to be oriented anteroposteriorly such that it cuts exactly through the middle of A2 segment (49,50) (*Figure 7A*). MPR also permits the segmental analysis of the MV leaflets by scanning the line of coaptation during systole to precisely identify the exact location of the prolapse and/or flail segments (*Figure 7B*). Common measurements performed with MPR for DMR include antero-posterior and commissural annular dimensions, leaflet length, prolapsing segment width, and septum to coaptation distance. The addition of CFD to MPR analysis enhances its capabilities in the more accurate diagnosis of the location and direction of the MR jet/s. This modality also facilitates in grading MR severity by measuring the 3D VCA (*Figure 7C*,*7D*). The 3D VCA has been validated as a reliable surrogate of the EROA in DMR.

Additional 3D TEE processing tools (iSlice, Philips Ultrasound Inc, Bothell, WA, USA) enable the transection of the MV in multiple tomographic planes perpendicular to the line of coaptation which can be displayed simultaneously. These techniques, combined with CFD, are extremely useful for segmental analysis of the location, origin and extension of the leaflet pathology (*Figure 8A,8B*).

Semiautomated quantification software uses 3D data sets to create parametric models of the MV. Although its clinical utility is limited in clinical practice, the valvular pathology displayed in the parametric image is simple to understand and is a useful teaching tool (*Figure 9A,9B*). In summary, 3D TEE enhances diagnosis, interpretation, clinical decision-making, and communication with the surgical team.

TEE in the post-bypass period is crucial in assessing the ventricular function, adequacy of repair, gradients, residual MR and SAM (3,9,20,51,52).

Biventricular systolic function may be depressed because of poor myocardial protection. Transient decrease in function, especially of the right ventricle, may result from air embolization (9). In a study by the Mayo Clinic group, one in five patients with a normal preoperative ejection fraction (EF) (>60%) undergoing MVR for DMR

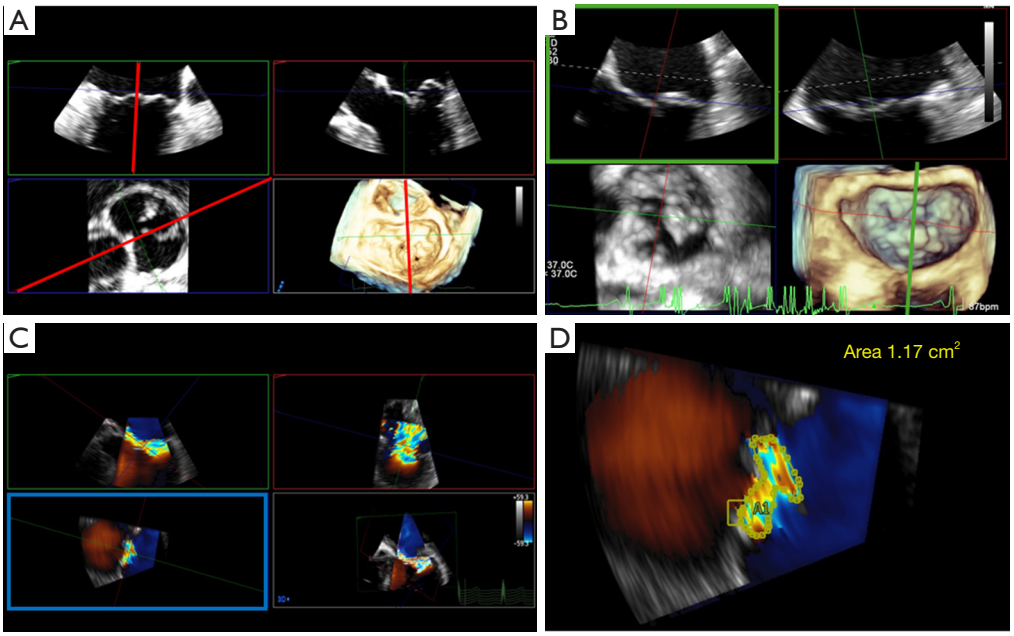

Figure 7 Multiplanar reconstruction of the mitral valve. (A) 3D TEE MPR showing three 2D images (mid-esophageal mitral commissural view, inverted mid-esophageal long-axis view, and en-face mitral valve view) and one 3D rendered-image (surgical view). The red plane transects the mitral valve exactly through the middle of A2-P2. (B) 3D TEE live MPR demonstrating prolapse of P2. The green line transects though P2. The green square shows the presence of P2 prolapse. (C) 3D TEE MPR with color flow Doppler demonstrating mitral regurgitation. (D) 3D TEE MPR with color flow Dopler measuring the 3D vena contracta area of the jet of mitral regurgitation. 2D, two-dimensional; 3D, three-dimensional; MRP, multiplanar reconstruction; TEE, transesophageal echocardiography.

demonstrated early dysfunction (EF <50%). Early decreases of up to 10% in EF can be explained as a volumetric adjustment after correction of the RV. Larger decreases in EF were attributed to the chronicity of MR, resulting in myocardial fibrosis, compensatory hypertrophy, and reverse remodeling (53).

Regional ischemia of the basal and mid inferolateral wall of the LV can result from distortion or occlusion of the LCX during MVS. If unrecognized or untreated ischemia may progress to infarction (*Video 4*). The LCX can lie as close as 1 mm to the posterior annulus (4,5) and is closer to the annulus with a left dominant coronary circulation than right or codominant posing a greater risk. TEE plays a key role in guiding therapy for hemodynamic management in the post CPB period.

Residual MR (RMR) of more than mild regurgitation (>+2) may be an indication to revise the repair (52,54,55). RMR can be attributed to unrepaired partial clefts, residual prolapse, excessive leaflet restriction, regional ischemia, SAM, iatrogenic perforations during suturing of the annuloplasty band (9) and inadequate coaptation length (<8 mm) (56) (*Figure 10*). 3D echocardiography is superior to 2D assessment for demonstrating the cause of the residual MR. Color 3D is very helpful in locating jets after MR repair. CFD is valuable in detecting severity and jet direction of the jet. Vena contracta measurements of >5 mm are considered moderate/severe, whereas VC <3 mm is considered mild (52).

MVR techniques with annuloplasty result in a reduction of the mitral valve area (MVA) and mild mitral stenosis (MS). A mean pressure gradient (MPG) ≤6 mmHg and/or a MVA ≥1.8 cm^2 is considered acceptable (52). Intraoperative transmitral peak and MPG ≥17 and ≥7 mmHg are suggestive of significant MS and may require reoperation (57). In DMR, MVR results in a small increase in the MPG and post-MVR MS is extremely rare. Intraoperative and postoperative gradients demonstrate a good correlation, which may increase or decrease slightly over time (58,59).

SAM, with or without left ventricular outflow tract obstruction (LVOTO), is a unique complication associated with MVR (*Video 5*). Intraoperative TEE is crucial in defining patients at risk for SAM post repair, detection of

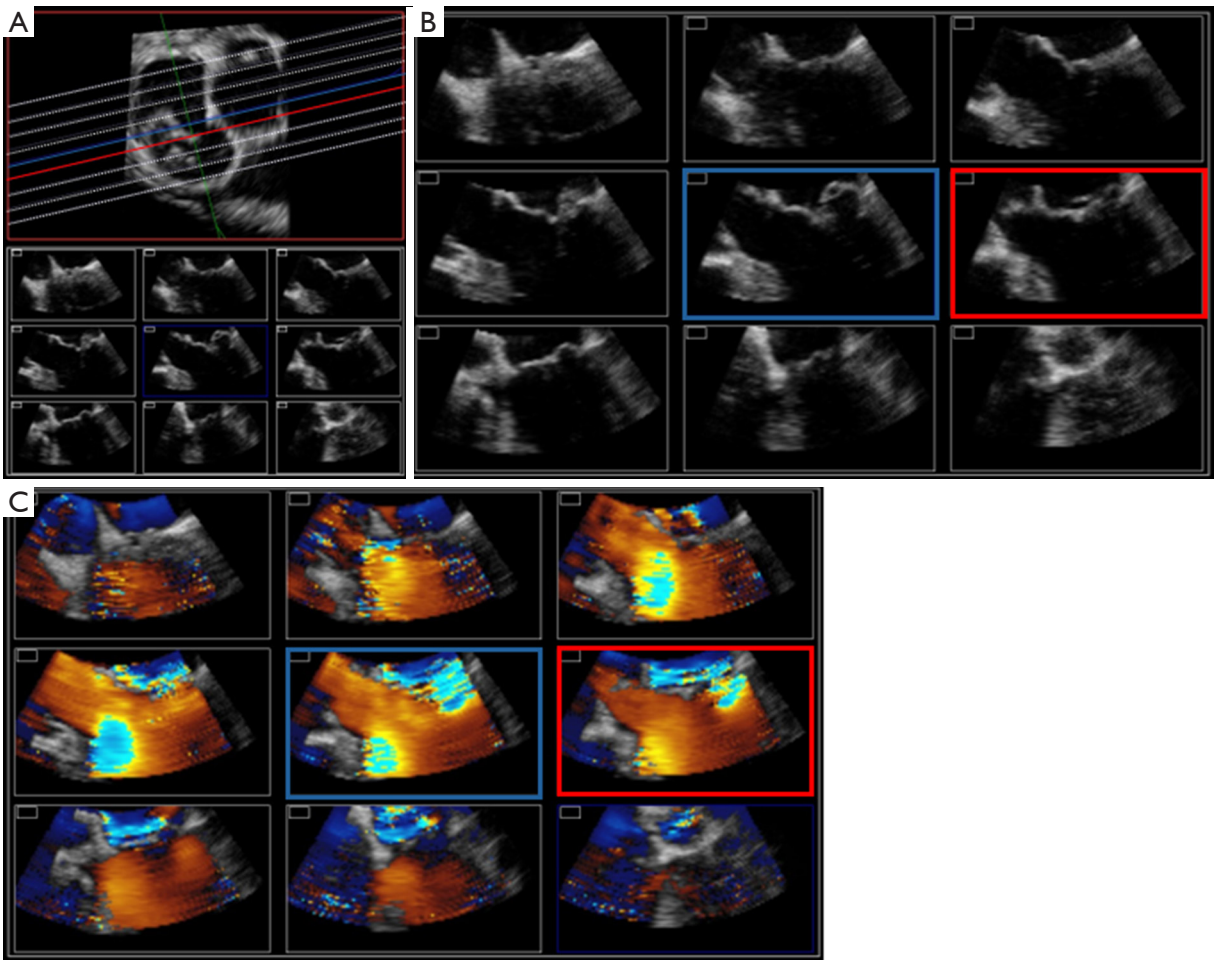

Figure 8 Three-dimensional transesophageal echocardiography volume slicing of the MV. (A) The MV is transected in multiple anteroposterior parallel planes from the lateral to the medial aspect of the mitral valve annulus (white, dotted lines in top image). (B) The tomographic planes are shown simultaneously on display. The blue and red squares show the exact location of the prolapse and flail at the medial aspect of the middle scallop of the posterior mitral leaflet (P3 side of P2). The blue and red squares correspond with the blue and red lines in the top image in (A). (C) Volume slicing with color flow Doppler. The blue and red squares show the exact origin of the jet of mitral regurgitation at the medial aspect of the middle scallop of the posterior mitral leaflet (P3 side of P2). MV, mitral valve.

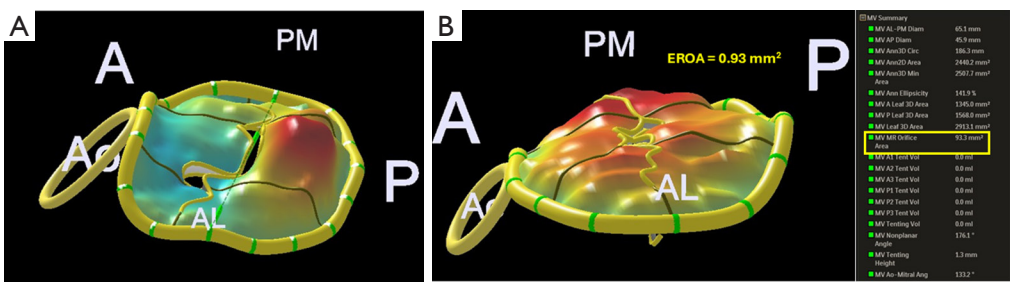

Figure 9 Parametric models of the mitral valve. (A) 3D TEE parametric model of the mitral valve, demonstrating a flail middle scallop (P2) of the posterior leaflet. (B) 3D TEE parametric model of the mitral valve, showing bileaflet prolapse. The red color represents leaflet tissue that is located above the annular plane during systole due to prolapse or flail. 3D, three-dimensional; A, anterior; AL, anterolateral; EROA, effective regurgitant orifice area; MV, mitral valve; P, posterior; PM, posteromedial; TEE, transesophageal echocardiography.

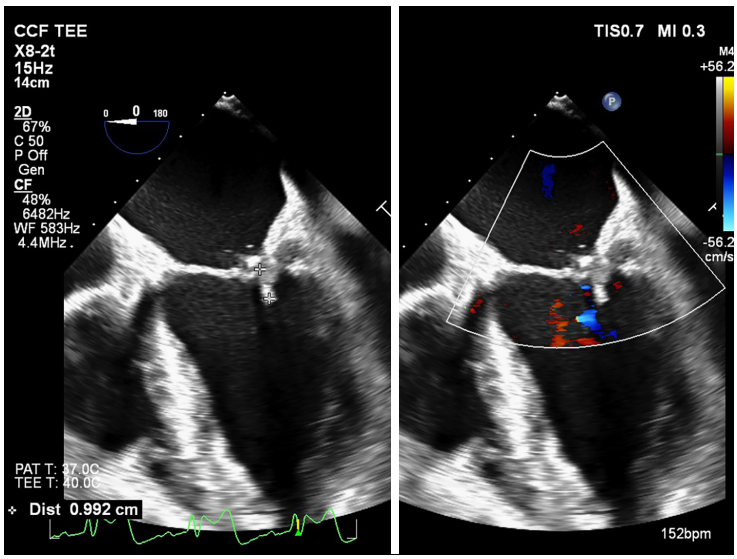

Figure 10 Post repair coaptation length.

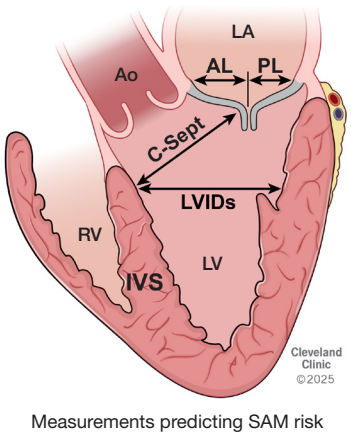

Figure 11 Echocardiographic predictors of post-repair SAM. AL, anterior leaflet; Ao, aorta; C-Sept, coaptation to septal distance; IVS, interventricular septum; LA, left atrium; LV, left ventricle; LVIDs, left ventricular internal diameter; PL, posterior leaflet; RV, right ventricle; SAM, systolic anterior motion.

SAM, extent and severity of SAM, LVOTO and resultant hemodynamic compromise, associated severity of MR, response to medical therapy, and the need for surgical intervention (9,52). Patients with a small (end diastolic diameter <45 mm), underfilled hyperdynamic ventricle, basal interventricular septal thickness >15 mm, a coaptation point to septal distance of <25 mm, a narrow mitral aortic angle <120°, anteriorly displaced papillary muscles, ratio of the anterior to posterior leaflet ≤1.3, and posterior leaflet length >15 mm, are considered at a higher risk for post-repair SAM (*Figure 11*). Inadequate resection of the posterior leaflet length to less than 15 mm and insertion of a smaller annuloplasty ring may increase the risk of post repair SAM (60-62). SAM after MVR is more commonly seen with DMR and the incidence is lower with the use of an incomplete annuloplasty band compared to a complete ring. Incorporating these predictors while tailoring a repair strategy can be important in preventing post repair SAM. For patients with excessive redundant leaflet tissue a sliding annuloplasty or folding plasty with concomitant use of neo chordae, with a resultant height of the posterior leaflet <15 mm can prevent SAM (62). A complete ring eliminates the posterior movement of the anterior leaflet thereby limiting systolic expansion of the LVOT increasing the susceptibility to SAM (63). A concomitant septal myectomy can prevent SAM in patients with basal septal hypertrophy (64). An edge-to-edge suture to limit the excursion of the anterior leaflet has been successfully used both prophylactically in patients at increased risk and as a remedy for repair-associated SAM. Edge-to-edge repair is associated with higher peak and mean trans mitral gradients as compared to conventional repair (65). Implementation of these strategies based on echocardiographic predictors has reduced the incidence of post-repair SAM to 4% (63). The pathophysiology of post-repair SAM is similar to SAM associated with HOCM. The

annuloplasty ring critically reduces the anteroposterior diameter and the mitral aortic angle with the coaptation zone positioned more anteriorly in a subaortic position. As systole progresses from the isovolumic to ejection phase, the anterior leaflet is progressively pushed towards the septum, resulting in LVOTO in a hyperdynamic ventricle (66-68). Discontinuation of inotropic support, administration of a β blocker, vasopressors and volume expansion can reduce SAM in most patients. Surgical intervention is considered if medical management fails, which includes an edge-to-edge suture, posterior leaflet reduction, shortening of the neochordae, or sliding annuloplasty with an upsized ring (61).

In summary, echocardiography plays a vital role throughout the perioperative course for MVR.

Acknowledgments

None.

Footnote

Funding: None.

Conflicts of Interest: The authors have no conflicts of interest to declare.

References

1. Duran CM. TEE: the 'roadmap' for mitral valve repair. J Heart Valve Dis 2006;15:521-3.
2. Silbiger JJ, Bazaz R. Contemporary insights into the functional anatomy of the mitral valve. Am Heart J 2009;158:887-95.
3. Adams DH, Anyanwu AC, Sugeng L, et al. Degenerative mitral valve regurgitation: surgical echocardiography. Curr Cardiol Rep 2008;10:226-32.
4. Ender J, Singh R, Nakahira J, et al. Echo didactic: visualization of the circumflex artery in the perioperative setting with transesophageal echocardiography. Anesth Analg 2012;115:22-6.
5. Coutinho GF, Leite F, Antunes MJ. Circumflex artery injury during mitral valve repair: Not well known, perhaps not so infrequent-lessons learned from a 6-case experience. J Thorac Cardiovasc Surg 2017;154:1613-20.
6. Hill AC, Bansal RC, Razzouk AJ, et al. Echocardiographic recognition of iatrogenic aortic valve leaflet perforation. Ann Thorac Surg 1997;64:684-9.
7. Maslow A. Mitral valve repair: an echocardiographic review: part 1. J Cardiothorac Vasc Anesth 2015;29:156-77.
8. Hahn RT, Abraham T, Adams MS, et al. Guidelines for performing a comprehensive transesophageal echocardiographic examination: recommendations from the American Society of Echocardiography and the Society of Cardiovascular Anesthesiologists. J Am Soc Echocardiogr 2013;26:921-64.
9. Sidebotham DA, Allen SJ, Gerber IL, et al. Intraoperative transesophageal echocardiography for surgical repair of mitral regurgitation. J Am Soc Echocardiogr 2014;27:345-66.
10. Adams DH, Rosenhek R, Falk V. Degenerative mitral valve regurgitation: best practice revolution. Eur Heart J 2010;31:1958-66.
11. Quill JL, Hill AJ, Laske TG, et al. Mitral leaflet anatomy revisited. J Thorac Cardiovasc Surg 2009;137:1077-81.
12. Anyanwu AC, Adams DH. Etiologic classification of degenerative mitral valve disease: Barlow's disease and fibroelastic deficiency. Semin Thorac Cardiovasc Surg 2007;19:90-6.
13. Carpentier A. Cardiac valve surgery--the "French correction". J Thorac Cardiovasc Surg 1983;86:323-37.
14. Antoine C, Mantovani F, Benfari G, et al. Pathophysiology of Degenerative Mitral Regurgitation: New 3-Dimensional Imaging Insights. Circ Cardiovasc Imaging 2018;11:e005971.
15. De Bonis M, Al-Attar N, Antunes M, et al. Surgical and interventional management of mitral valve regurgitation: a position statement from the European Society of Cardiology Working Groups on Cardiovascular Surgery and Valvular Heart Disease. Eur Heart J 2016;37:133-9.
16. Zoghbi WA, Adams D, Bonow RO, et al. Recommendations for Noninvasive Evaluation of Native Valvular Regurgitation: A Report from the American Society of Echocardiography Developed in Collaboration with the Society for Cardiovascular Magnetic Resonance. J Am Soc Echocardiogr 2017;30:303-71.

17. Ring L, Rana BS, Ho SY, et al. The prevalence and impact of deep clefts in the mitral leaflets in mitral valve prolapse. Eur Heart J Cardiovasc Imaging 2013;14:595-602.
18. Mantovani F, Clavel MA, Vatury O, et al. Cleft-like indentations in myxomatous mitral valves by three-dimensional echocardiographic imaging. Heart 2015;101:1111-7.
19. Mahmood F, Sharkey A, Maslow A, et al. Echocardiographic Assessment of the Mitral Valve for Suitability of Repair: An Intraoperative Approach From a Mitral Center. J Cardiothorac Vasc Anesth 2022;36:2164-76.
20. Ender J, Sgouropoulou S. Value of transesophageal echocardiography (TEE) guidance in minimally invasive mitral valve surgery. Ann Cardiothorac Surg 2013;2:796-802.
21. Coddens J, Deloof T, Hendrickx J, et al. Transesophageal echocardiography for port-access surgery. J Cardiothorac Vasc Anesth 1999;13:614-22.
22. Gillinov M, Burns DJP, Wierup P. The 10 Commandments for Mitral Valve Repair. Innovations (Phila) 2020;15:4-10.
23. Obase K, Jeevanandam V, Saito K, et al. Visualization and measurement of mitral valve chordae tendineae using three-dimensional transesophageal echocardiography from the transgastric approach. J Am Soc Echocardiogr 2015;28:449-54.
24. Stewart WJ, Currie PJ, Salcedo EE, et al. Evaluation of mitral leaflet motion by echocardiography and jet direction by Doppler color flow mapping to determine the mechanisms of mitral regurgitation. J Am Coll Cardiol 1992;20:1353-61.
25. Rehfeldt KH, Click RL, Orszulak TA. Regurgitant jet direction in patients with prolapse of the anterolateral scallop of the posterior mitral valve leaflet. J Cardiothorac Vasc Anesth 2007;21:581-3.
26. Lancellotti P, Moura L, Pierard LA, et al. European Association of Echocardiography recommendations for the assessment of valvular regurgitation. Part 2: mitral and tricuspid regurgitation (native valve disease). Eur J Echocardiogr 2010;11:307-32.
27. Iglesias I. Intraoperative TEE assessment during mitral valve repair for degenerative and ischemic mitral valve regurgitation. Semin Cardiothorac Vasc Anesth 2007;11:301-5.
28. Shiran A, Merdler A, Ismir E, et al. Intraoperative transesophageal echocardiography using a quantitative dynamic loading test for the evaluation of ischemic mitral regurgitation. J Am Soc Echocardiogr 2007;20:690-7.
29. Chen CG, Thomas JD, Anconina J, et al. Impact of impinging wall jet on color Doppler quantification of mitral regurgitation. Circulation 1991;84:712-20.
30. Hall SA, Brickner ME, Willett DL, et al. Assessment of mitral regurgitation severity by Doppler color flow mapping of the vena contracta. Circulation 1997;95:636-42.
31. Goebel B, Heck R, Hamadanchi A, et al. Vena contracta area for severity grading in functional and degenerative mitral regurgitation: a transoesophageal 3D colour Doppler analysis in 500 patients. Eur Heart J Cardiovasc Imaging 2018;19:639-46.
32. Lambert AS. Proximal isovelocity surface area should be routinely measured in evaluating mitral regurgitation: a core review. Anesth Analg 2007;105:940-3.
33. Enriquez-Sarano M, Seward JB, Bailey KR, et al. Effective regurgitant orifice area: a noninvasive Doppler development of an old hemodynamic concept. J Am Coll Cardiol 1994;23:443-51.
34. Enriquez-Sarano M, Dujardin KS, Tribouilloy CM, et al. Determinants of pulmonary venous flow reversal in mitral regurgitation and its usefulness in determining the severity of regurgitation. Am J Cardiol 1999;83:535-41.
35. Itakura K, Utsunomiya H, Takemoto H, et al. Prevalence, distribution, and determinants of pulmonary venous systolic flow reversal in severe mitral regurgitation. Eur Heart J Cardiovasc Imaging 2021;22:964-73.
36. Applebaum RM, Cutler WM, Bhardwaj N, et al. Utility of transesophageal echocardiography during port-access minimally invasive cardiac surgery. Am J Cardiol 1998;82:183-8.
37. Sorrell VL, Rajeev AG, Nifong LW, et al. Intraoperative transesophageal echocardiography with a special focus on a patient undergoing advanced robotic-assisted procedures. Echocardiography 2002;19:583-7.
38. Lewis CT, Stephens RL, Tyndal CM, et al. Concomitant robotic mitral and tricuspid valve repair: technique and early experience. Ann Thorac Surg 2014;97:782-7.
39. Vernick W, Atluri P. Robotic and minimally invasive cardiac surgery. Anesthesiol Clin 2013;31:299-320.
40. Deshpande SP, Lehr E, Odonkor P, et al. Anesthetic management of robotically assisted totally endoscopic coronary artery bypass surgery (TECAB). J Cardiothorac Vasc Anesth 2013;27:586-99.
41. Labriola C, Greco F, Braccio M, et al. Percutaneous Coronary Sinus Catheterization With the ProPlege Catheter Under Transesophageal Echocardiography and Pressure Guidance. J Cardiothorac Vasc Anesth 2015;29:598-604.

42. Hanada S, Sakamoto H, Swerczek M, et al. Initial experience with percutaneous coronary sinus catheter placement in minimally invasive cardiac surgery in an academic center. BMC Anesthesiol 2016;16:33.
43. Labriola C, Paparella D, Labriola G, et al. Reliability of Percutaneous Pulmonary Vent and Coronary Sinus Cardioplegia in the Setting of Minimally Invasive Aortic Valve Replacement: A Single-Center Experience. J Cardiothorac Vasc Anesth 2017;31:1203-9.
44. Lang RM, Badano LP, Tsang W, et al. EAE/ASE recommendations for image acquisition and display using three-dimensional echocardiography. Eur Heart J Cardiovasc Imaging 2012;13:1-46.
45. Ben Zekry S, Nagueh SF, Little SH, et al. Comparative accuracy of two- and three-dimensional transthoracic and transesophageal echocardiography in identifying mitral valve pathology in patients undergoing mitral valve repair: initial observations. J Am Soc Echocardiogr 2011;24:1079-85.
46. Tsang W, Lang RM. Three-dimensional echocardiography is essential for intraoperative assessment of mitral regurgitation. Circulation 2013;128:643-52; discussion 652.
47. Biaggi P, Gruner C, Jedrzkiewicz S, et al. Assessment of mitral valve prolapse by 3D TEE angled views are key. JACC Cardiovasc Imaging 2011;4:94-7.
48. Wollborn J, Schuler A, Sheu RD, et al. Real-Time Multiplanar Reconstruction Imaging Using 3-Dimensional Transesophageal Echocardiography in Structural Heart Interventions. J Cardiothorac Vasc Anesth 2023;37:570-81.
49. Geyer M, Sotiriou E, Tamm AR, et al. Advanced Protocol for Three-Dimensional Transesophageal Echocardiography Guidance Implementing Real-Time Multiplanar Reconstruction for Transcatheter Mitral Valve Repair by Direct Annuloplasty. J Am Soc Echocardiogr 2019;32:1359-65.
50. Hien MD, Rauch H, Lichtenberg A, et al. Real-time three-dimensional transesophageal echocardiography: improvements in intraoperative mitral valve imaging. Anesth Analg 2013;116:287-95.
51. Zamper R, Prempeh A, Iglesias I, et al. Intraoperative transesophageal echocardiography following mitral valve repair: a systematic review. Braz J Anesthesiol 2022;72:379-97.
52. Maslow A. Mitral valve repair: an echocardiographic review: Part 2. J Cardiothorac Vasc Anesth 2015;29:439-71.
53. Quintana E, Suri RM, Thalji NM, et al. Left ventricular dysfunction after mitral valve repair--the fallacy of "normal" preoperative myocardial function. J Thorac Cardiovasc Surg 2014;148:2752-60.
54. Fix J, Isada L, Cosgrove D, et al. Do patients with less than 'echo-perfect' results from mitral valve repair by intraoperative echocardiography have a different outcome? Circulation 1993;88:II39-48.
55. Bhudia SK, McCarthy PM, Smedira NG, et al. Edge-to-edge (Alfieri) mitral repair: results in diverse clinical settings. Ann Thorac Surg 2004;77:1598-606.
56. Yamauchi T, Taniguchi K, Kuki S, et al. Evaluation of the mitral valve leaflet morphology after mitral valve reconstruction with a concept "coaptation length index". J Card Surg 2004;19:535-8.
57. Riegel AK, Busch R, Segal S, et al. Evaluation of transmitral pressure gradients in the intraoperative echocardiographic diagnosis of mitral stenosis after mitral valve repair. PLoS One 2011;6:e26559.
58. Goldberger MI, Pollak A, Fuller M, et al. Transmitral Pressure Gradients in Patients With Degenerative Mitral Regurgitation After Robotic Mitral Valve Repair With Leaflet Preservation Techniques. Echocardiography 2024;41:e70001.
59. Murashita T, Greason KL, Suri RM, et al. Mitral valve gradient after valve repair of degenerative regurgitation with restrictive annuloplasty. J Thorac Cardiovasc Surg 2016;151:106-9.
60. Maslow AD, Regan MM, Haering JM, et al. Echocardiographic predictors of left ventricular outflow tract obstruction and systolic anterior motion of the mitral valve after mitral valve reconstruction for myxomatous valve disease. J Am Coll Cardiol 1999;34:2096-104.
61. Alfieri O, Lapenna E. Systolic anterior motion after mitral valve repair: where do we stand in 2015? Eur J Cardiothorac Surg 2015;48:344-6.
62. Varghese R, Itagaki S, Anyanwu AC, et al. Predicting systolic anterior motion after mitral valve reconstruction: using intraoperative transoesophageal echocardiography to identify those at greatest risk. Eur J Cardiothorac Surg 2014;45:132-7; discussion 137-8.
63. Loulmet DF, Yaffee DW, Ursomanno PA, et al. Systolic anterior motion of the mitral valve: a 30-year perspective. J Thorac Cardiovasc Surg 2014;148:2787-93.
64. Said SM, Schaff HV, Suri RM, et al. Bulging subaortic septum: an important risk factor for systolic anterior motion after mitral valve repair. Ann Thorac Surg 2011;91:1427-32.
65. Myers PO, Khalpey Z, Maloney AM, et al. Edge-to-

edge repair for prevention and treatment of mitral valve systolic anterior motion. J Thorac Cardiovasc Surg 2013;146:836-40.
66. Jebara VA, Mihaileanu S, Acar C, et al. Left ventricular outflow tract obstruction after mitral valve repair. Results of the sliding leaflet technique. Circulation 1993;88:II30-4.
67. Jiang L, Levine RA, King ME, et al. An integrated mechanism for systolic anterior motion of the mitral valve in hypertrophic cardiomyopathy based on echocardiographic observations. Am Heart J 1987;113:633-44.
68. Hagège AA, Bruneval P, Levine RA, et al. The mitral valve in hypertrophic cardiomyopathy: old versus new concepts. J Cardiovasc Transl Res 2011;4:757-66.

Cite this article as: Mehta AR, Burbano-Vera N. Intraoperative transesophageal echocardiography: the roadmap for successful mitral valve repair. Ann Cardiothorac Surg 2026;15(1):3. doi: 10.21037/acs-2025-dmv-10